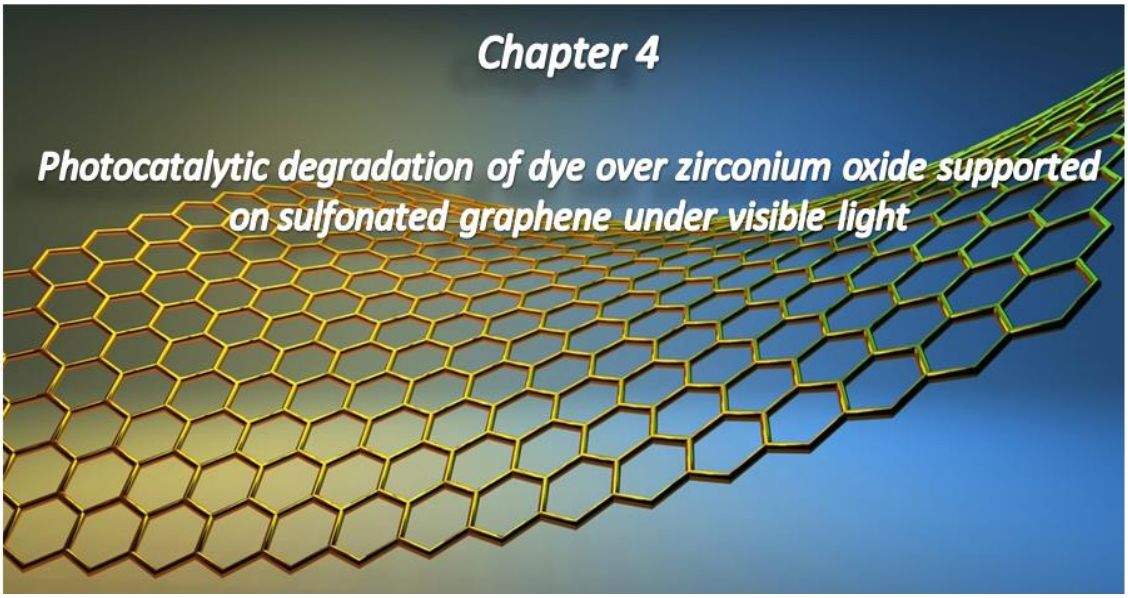

GRAPHICAL ABSTRACT

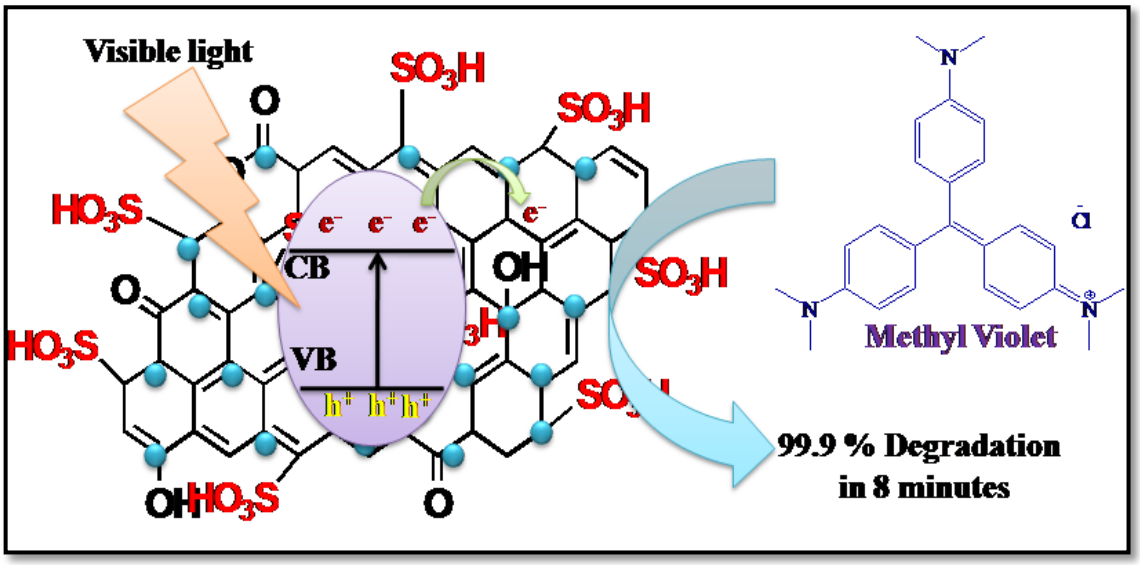

Monoclinic ZrO_2 supported on sulfonated graphene possesses higher photo-catalytic activity compared to SG and *m*-ZrO_2/rGO under visible light towards degradation of methyl violet dye.

4.1 Introduction

With a rapidly growing population, urbanization and industrialization, the environmental pollution is becoming increasingly serious. Various techniques are used for water decontamination like adsorption [1, 2], coagulation [3], biodegradation [4] and photocatalysis [5-7]. In comparison to these techniques, photocatalytic degradation is considered as the most high-efficient and promising method as it is economic and can completely oxidizes the organic pollutants to water and carbondioxide [8, 9].

There are number of metal oxide and sulfide semiconductor materials used as photocatalyst for photocatalytic degradation such as TiO_2, ZrO_2, ZnO, WO_3, Fe_2O_3, V_2O_5, Nb_2O_5, $SrTiO_3$, ZnS and CdS [10,11]. Among them, ZrO_2 has been considered as an important metal oxide because of its numerous unique properties that makes it versatile for a wide range of applications. Due to its environmental friendly nature with less toxicity, high chemical inertness, biocompatibility, cost effectiveness with good thermal stability and electrochemical properties it can be successfully applied as catalyst, catalyst supports, dielectric materials, high-performance ceramic materials, fuel cells, as well as photocatalytic materials [12-20]. It has been considered as an efficient photocatalyst in various photochemical reactions such as water purification and water splitting because of its relatively wide band gap value and high negative value of the conduction band. The reported band gap value of ZrO_2 range was 3.25 to 5.1 eV depending on the phase and synthetic approaches [21-23].

The use of ZrO_2 as an efficient photocatalyst requires a good manipulation of its morphology, porous structure and crystallinity development. ZrO_2 possesses three well known polymorphs: cubic, monoclinic and tetragonal. Out of these the pure monoclinic phase ZrO_2 having the lowest band gap value has highest photocatalytic activity. The highest photocatalytic activity of the monoclinic ZrO_2 can be attributed to the combined effects of high crystallinity, large pore sizes, high density of surface hydroxyl groups and the presence of small amount of oxygen-deficient zirconium oxide phase [24]. Due to its wide band gap ZrO_2 can absorbs only UV light which comprises a minimum fraction (~4%) of solar energy. Modification of ZrO_2 by doping or compounding carbon nanomaterials can enhance its photocatalytic activity under visible light [25].

Among various carbon nanomaterials, graphene based photocatalysts have attracted extensive attention because of their unique electronic and optical properties [26, 27]. The high electron mobility and conjugated structure of graphene make it as an ideal

electron acceptor and good electron transporting medium. Anchoring semiconductor nanoparticles on graphene sheets can decrease the electron-hole pair recombination and increase the absorptivity in the visible region. Graphene-based materials with enhanced photocatalytic efficiency can degrade both cationic and anionic organic dyes [28, 29]. Although graphene and nanoparticles should provide high surface-active sites due to the high van der Waals energy the graphene prone to aggregation, which hinders the interactions between graphene and nanoparticles [30, 31].

Sulfonated graphene (SG) is a functionalized graphene with p-phenyl-SO_3H groups covalently bonded to the graphene sheet surface as well as edges. SG is not only highly water-soluble but also has linear dispersed charge carrier travelling at nearly the speed of light and would be a photo-induced electron reservoir to transfer and separate electrons and holes [32-35]. Hence, it provides a great support to nanoparticles on the basis of preserving the functionality of graphene [36].

Incorporating ZrO_2 on graphene can enhanced the photocatalytic activity of ZrO_2. Rani et al. [37] has synthesized ZrO_2-graphene composite by using solution based method and studied their photocatalytic activity towards degradation of MO under UV-light. They have found that with increasing the concentration of graphene the photocatalytic activity of ZrO_2 increased. In another work, Gurushanta et al. [38] reported a green synthetic route for synthesis of ZrO_2-graphene composite and used as a photocatalyst for the degradation of RB 4 under sunlight.

To the best of our knowledge, no systematic study on the photocatalytic activity of monoclinic ZrO_2 supported on SG (*m*-ZrO_2/SG) has been carried out so far. So in this work, *m*-ZrO_2/SGE was synthesized by a simple solution based method. The photocatalytic degradation of methyl violet (MV) dye was studied by using SG, *m*-ZrO_2/rGO annealed at three different temperatures and *m*-ZrO_2/SG (annealed at 1200˚C) under visible light. It was found that the incorporation of *m*-ZrO_2 into rGO and SG has increased its photo-catalytic activity. The photo-catalytic activity of *m*-ZrO_2 further increased with increasing annealing temperatures. *m*-ZrO_2/SG photo-catalyst was observed to possess the highest catalytic efficiency amongst the other synthetic composites. The photo-catalyst can be recycled and reused after washing with absolute alcohol and DI water.

4.2 Experimental section

4.2.1 Chemicals

Graphite power (<20 micron) was purchased from Aldrich and used as received $NaNO_3$, conc. H_2SO_4, $KMnO_4$, H_2O_2 (30%), HCl, NaOH, hydrazine monohydrate, dichloro methane, chlorosulfonic acid, zirconium oxychloride octahydrate and methyl violet were procured from Merck.

4.2.2 Synthesis of SG and m-ZrO_2

SG was synthesized by sulfonation of rGO. rGO was prepared from natural graphite using modified Hummers method [39] followed by reduction as mentioned in Chapter 3. To prepare SG, 76 mg of graphene was dispersed in 30 mL dichloromethane by ultrasonication treatment. 10 mL of chlorosulfonic acid was added dropwise into the dispersion 0˚C. Then the reaction mixture was allowed to go up to the room temperature and held overnight. The reaction was stopped by neutralization with 20 % NaOH solution. The obtained precipitation was collected by filtration, washed with 1M HCl solution and DI water several times and dried at 80˚C [40].

To prepare *m*-ZrO_2, zirconium oxychloride octahydrate was dissolved in DI water zirconium hydroxide was precipitated by adding 2M NaOH dropwise (maintaining pH at 8.0) with constant stirring. The resulting precipitate was filtered and washed with DI and acetone several times and then dried at 100˚C overnight followed by calcination at three different temperatures (600˚C, 1000˚C and 1200˚C) for 2 h in furnace.

4.2.3 Synthesis of m-ZrO_2/Graphene (m-ZrO_2/rGO) and ZrO_2-sulfonated graphene (m-ZrO_2/SG) nanocomposites

The synthesized *m*-ZrO_2 calcined at three different temperatures and rGO were used as precursors to prepare *m*-ZrO_2/rGO. rGO dispersion was made in DI water by ultrasonication and *m*-ZrO_2 solution was prepared by dissolving *m*-ZrO_2 powder on dilute HCl solution. Then the two solutions were mixed and subjected to stirring for 12 h after 30 min ultranication treatment. The black colored product was filtered, washed with DI water and dried in oven at 80˚C.

m-ZrO_2/SG was synthesized from *m*-ZrO_2 (calcined at 1200˚C) and SG by following the same procedure.

4.2.4 Characterization

The prepared samples were characterized by using several analytical methods such as FTIR, XRD, Raman analysis, SEM and EDX analyses.

4.2.5 Evaluation of photocatalytic activity

The photocatalytic activity of the synthesized materials was investigated using the degradation of MV dye in an aqueous solution under visible light irradiation (200 W, LED light). Initially the photocatalysts were suspended in an aqueous solution of MV by using a magnetic stirrer. Prior to the degradation reaction is carried out; the suspended mixture was left in dark for 30 minutes to established the adsorption equilibrium. The reaction was started by irradiating the suspension by the light source placed at a distance of 10 cm at room temperature. The mixture was withdrawn periodically and centrifuged to separate the photocatalyst from the dispersion. The degradation was monitored by UV-Vis Spectrophotometer via recording the absorbance of characteristic peak of MV at 579.4 nm wavelength.

4.3 Results and discussion

4.3.1 FTIR analysis

Fig. 4.1 shows the FTIR spectrum of GO, SG, *m*-ZrO_2/$rGO_{1200^\circ C}$, and *m*-ZrO_2/$SG_{1200^\circ C}$. In the FTIR spectrum of GO (Fig. 4.1a), the peak at 3408.46 cm^{-1} is attributed to O-H bending vibrations, peak at 2930.24 cm^{-1} indicates C-H bending vibrations. The peak at 1731.34 cm^{-1} is attributed to C=O stretching in carbonyl or carboxyl moiety. The peak at 1623.03 cm^{-1} shows the C=C stretching vibrations. Peak at 1379.75 cm^{-1} is attributed to C-O bending and the peak at 1069.82 cm^{-1} is due to C-O stretching vibrations. In the FTIR spectrum of SG (Fig. 4.1b), the intensity of the peak due to carbonyl group at 1708.69 cm^{-1} decreases significantly, which indicate successful reduction of GO. The new peak appeared at 1158.89 cm^{-1} is attributed to S=O stretching vibrations which confirms formation of SG. In the FTIR spectrum of *m*-ZrO_2/$rGO_{1200^\circ C}$ (Fig. 4.1c), the peaks due to rGO appeared with little shifting along with some new peaks. The peak observed at 1555.75cm^{-1} is due to Zr-O stretching vibration. In the FTIR spectrum of *m*-ZrO_2/$SG_{1200^\circ C}$ (Fig. 4.1d) peaks correspond to both ZrO_2 and SG appears which indicates successful formation of *m*-ZrO_2/$SG_{1200^\circ C}$. The peaks for S=O group is

shifted from 1158.89 cm^{-1} to 1170.73cm^{-1} and Zr-O is shifted from 1555.75cm^{-1} to 1559.65cm^{-1} which is because of the π-π interactions between ZrO_2 and SG.

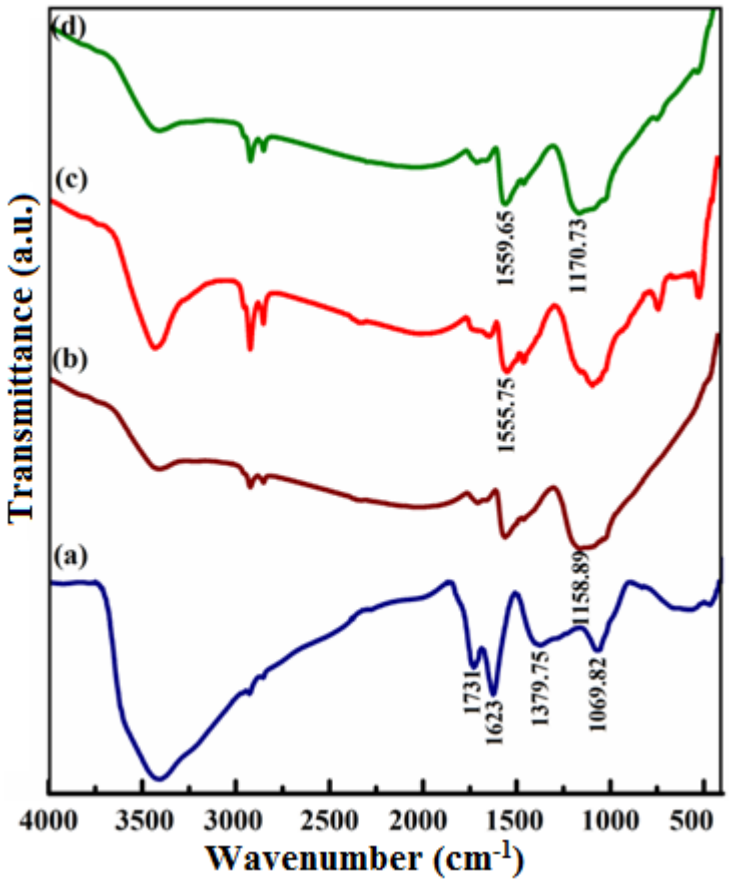

Fig. 4.1 FTIR spectrum of (a) GO, (b) SG, (c) *m*-ZrO_2/rGO $_{1200^{\circ}C}$, and (d) *m*-ZrO_2/SG $_{1200^{\circ}C}$.

4.3.2 XRD analysis

XRD analysis was carried out to identify the crystallinity of the samples. Fig.4.2 shows the XRD pattern of SG, *m*-ZrO_2/$rGO_{600^{\circ}C}$, *m*-ZrO_2/$rGO_{1000^{\circ}C}$, *m*-ZrO_2/$rGO_{1200^{\circ}C}$ and *m*-ZrO_2/$SG_{1200^{\circ}C}$. SG exhibits two broad peaks at 2θ=25.45° and 42.8° corresponds to the (002) and (100) planes (Fig.4.2a). In the XRD pattern of *m*-ZrO_2/$rGO_{600^{\circ}C}$ (Fig.4.2b), peaks observed at 2θ=28.06˚, 31.42˚, 33.95˚, 35.08˚, 38.36˚, 40.64˚, 44.81˚, 49.12˚, 50.12˚, 54.04˚, 55.44˚, 57.33˚, 59.86˚, 62.64˚ and 65.54˚ for the planes (111), (111), (002), (200), (012), (211), (112), (022), (220), (202), (013), (310), (131), (311) and (132) respectively, are due to monoclinic phase of ZrO_2 (JCPDS card no: 899066). A broad peak is observed at 2θ =24.29˚ for the presence of graphene in the composite. In the XRD spectra of *m*-ZrO_2/$rGO_{1000^{\circ}C}$ (Fig.4.2c), *m*-ZrO_2/rGO $_{1200^{\circ}C}$ (Fig.4.2 d) and *m*-ZrO_2/$SG_{1200^{\circ}C}$ (Fig.4.2e) peaks correspond to both ZrO_2 and rGO appeared while the

peak intensity of ZrO_2 increases with annealing temperature which is due to removal of absorbed molecules at higher temperature. Again, little shifting of the peaks occurred which is due to the interaction of ZrO_2 and graphene. In the XRD patterns of all the composites there are no peaks of cubic and tetragonal phases of ZrO_2. This confirms that the synthesized composites contain a single crystalline monoclinic phase ZrO_2 without any phase impurities. The intense sharp peaks of ZrO_2 confirm the formation of high crystalline ZrO_2 nanoparticles.

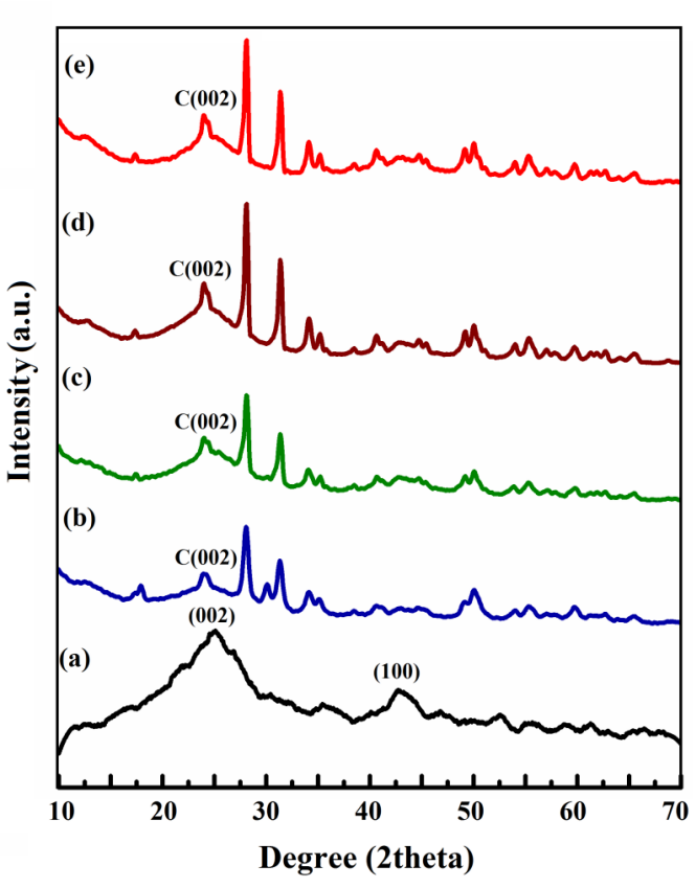

Fig. 4.2 XRD pattern of (a) SG, (b) *m*-ZrO_2/$rGO_{600^\circ C}$, (c) *m*-ZrO_2/$rGO_{1000^\circ C}$, (d) *m*-ZrO_2/$rGO_{1200^\circ C}$ and (e) *m*-ZrO_2/$SG_{1200^\circ C}$

4.3.3 Raman analysis

Raman spectra of (a) rGO, (b) SG, (c) *m*-ZrO_2/$rGO_{1200^\circ C}$ and (d) *m*-ZrO_2/$SG_{1200^\circ C}$ are shown in Fig.4.3. The D band G band and the peak intensity between these two bands (I_D/I_G) are shown in table 4.1. The D band arises from defect structure, and the G band is related to the vibration of sp^2 carbon. It is observed that, I_D/I_G ratio of *m*-ZrO_2/$rGO_{1200^\circ C}$ is less than that of rGO which indicates the successful incorporation of $ZrO_{2\ (1200^\circ C)}$ into the rGO structure respectively. Also the I_D/I_G ratio of *m*-ZrO_2/$SG_{1200^\circ C}$ is less than that of

SG which indicates the successful incorporation of $ZrO_{2\ (1200^{\circ}C)}$ into the SG. The shifting of the D and G band indicates the π-π interaction among each material in the composites.

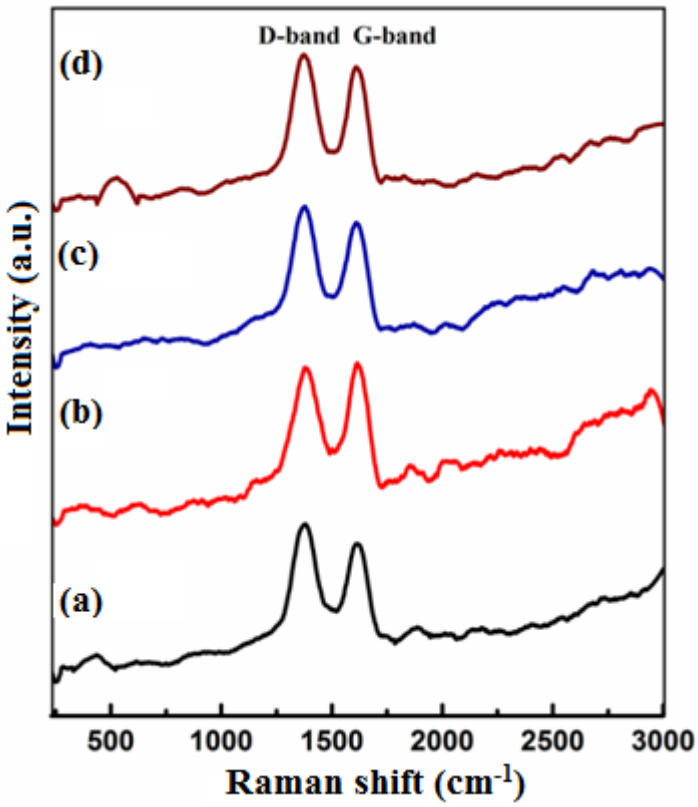

Fig. 4.3 Raman spectra of (a) rGO, (b) SG, (c) *m*-ZrO_2/$rGO_{1200^{\circ}C}$ and (d) *m*-ZrO_2/$SG_{1200^{\circ}C}$.

Table 4.1 Raman spectral data

Composites	D-band (cm^{-1})	G-band (cm^{-1})	I_D/I_G ratio
rGO	1377.80	1621.61	1.10
SG	1375.97	1604.58	1.01
***m*-ZrO_2/$rGO_{200^{\circ}C}$**	1375.97	1604.58	1.09
***m*-ZrO_2/$SG_{1200^{\circ}C}$**	1368.19	1611.58	1.07

4.3.4 SEM and EDX analysis

The surface morphology and the elements present in the synthesized nanocomposites were studied by using SEM and EDX analyses, respectively. Fig.4.4 shows the SEM images of rGO, ZrO_2, *m*-ZrO_2/$rGO_{1200^{\circ}C}$ and *m*-ZrO_2/$SG_{1200^{\circ}C}$. The SEM image of rGO shows the crumple, layered structure while the ZrO_2 nanoparticles show spherical structure. SEM images of *m*-ZrO_2/$rGO_{1200^{\circ}C}$ and *m*-ZrO_2/$SG_{1200^{\circ}C}$ show that the

layered structure of graphene become rough due to surface functionalization. The nanosized particles of ZrO_2 seen to be dispersed on the layers graphene and sulfonated graphene.

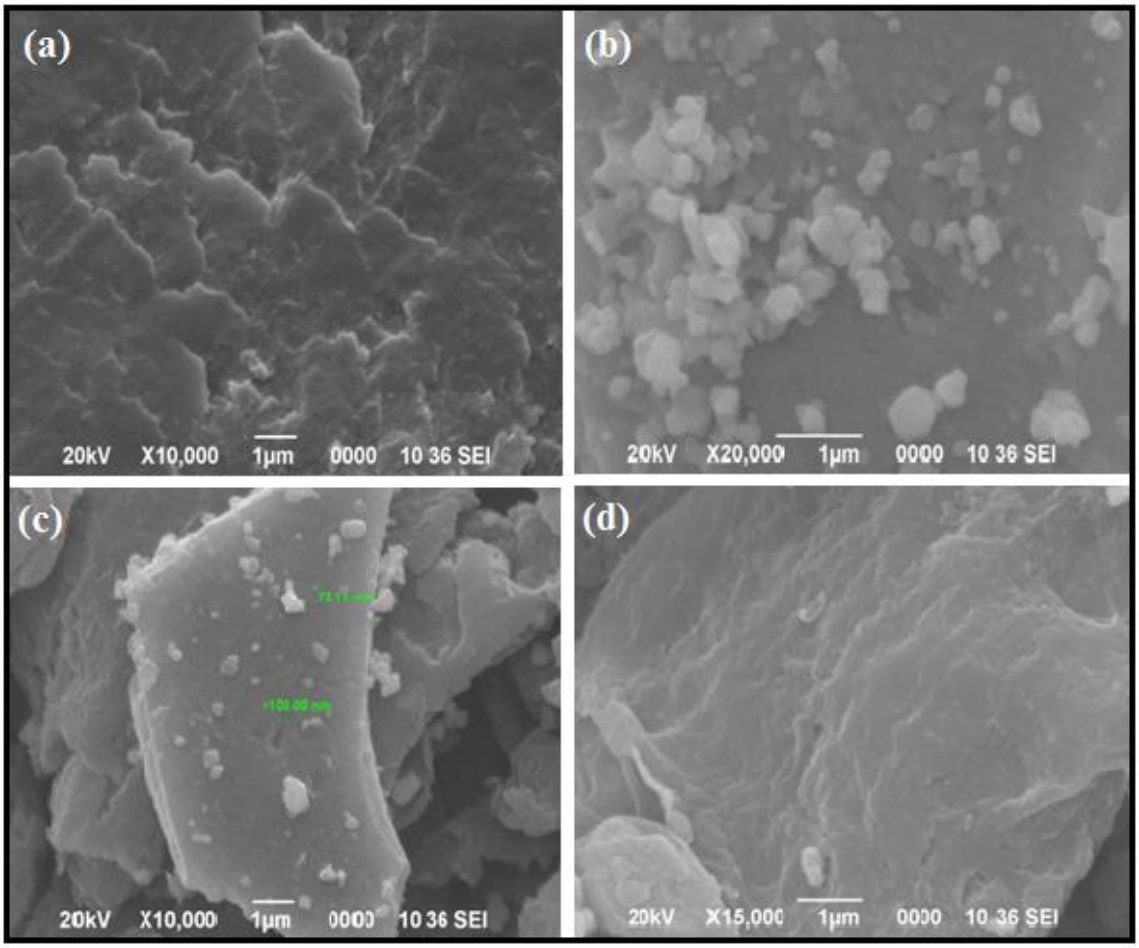

Fig. 4.4 SEM image of (a) rGO, (b) ZrO_2 (c) *m*-ZrO_2/$rGO_{1200^{\circ}C}$ and (d) *m*-ZrO_2/$rGO_{1200^{\circ}C}$

Fig.4.5 shows the EDX analysis of *m*-ZrO_2/$rGO_{1200^{\circ}C}$ and *m*-ZrO_2/$SG_{1200^{\circ}C}$. Fig.4.5a confirms the presence of Zr, C and O in the *m*-ZrO_2/$rGO_{1200^{\circ}C}$ nanocomposite and Fig.4.5b confirms the presence of Zr, C, O and S in the *m*-ZrO_2/$SG_{1200^{\circ}C}$ nanocomposite.

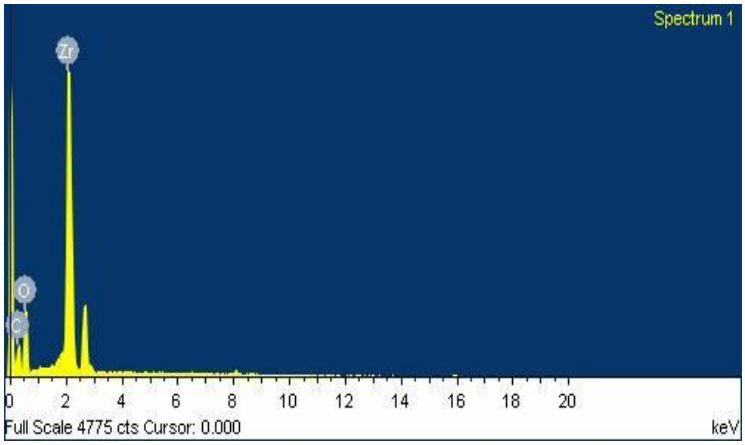

Fig. 4.5(a) EDX analysis of *m*-ZrO_2/$rGO_{1200^{\circ}C}$

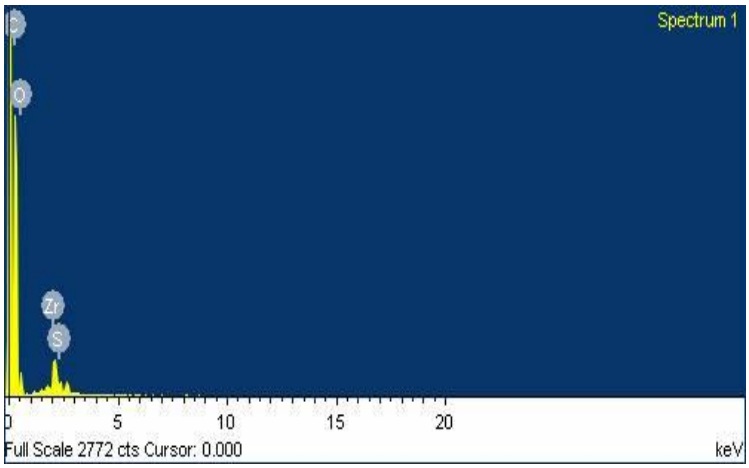

Fig.4.5(b) EDX analysis *m*-ZrO_2/$SG_{1200^{\circ}C}$

4.3.5 Photocatalytic activity analysis

Degradation factor (X) can be calculated by using the following equation:

$$X= (C_0-C)/ C_0$$

Where, C_0 is the initial dye concentration and C is the concentration of dye at any time.

The degradation of the MV dye without any catalyst is shown in the Fig.4.6a. In the absence of catalyst no degradation is observed. However, in presence of SG as catalyst, complete photo-degradation of the dye takes place after 105 minutes as shown in Fig.4. 6b. The spectrums were taken after every five minutes of the reaction under irradiation of light. It was observed that the concentration of MV decreases gradually with increase in duration of irradiation time.

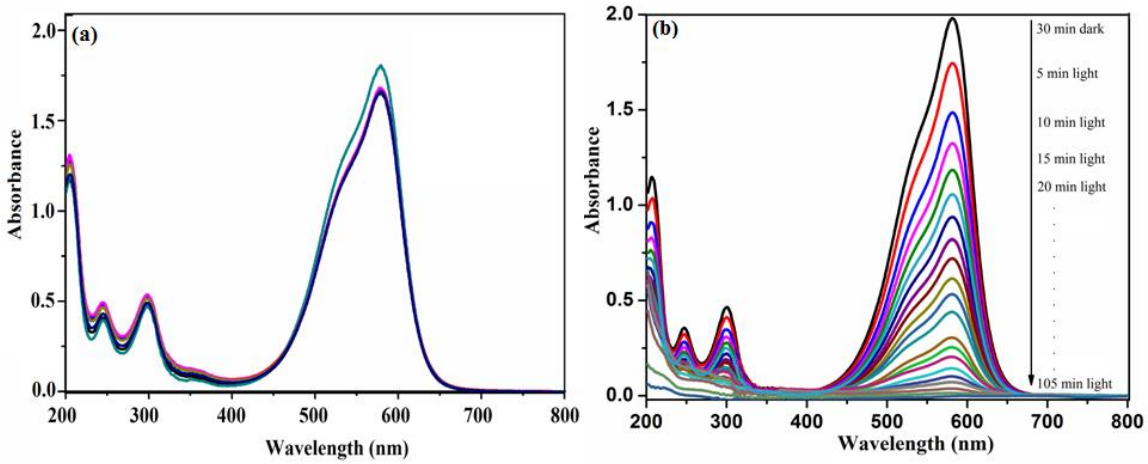

Fig.4.6 UV-vis spectrum of the dye after treatment in visible light (a) in absence of catalyst, (b) in presence of SG

Fig. 4.7 shows the degradation factor versus time variation. In absence of any catalyst the degradation factor remains almost same even upto 60 minutes (Fig.4.7a) and in presence of SG the degradation factor increases with increase in time (Fig.4.7b).

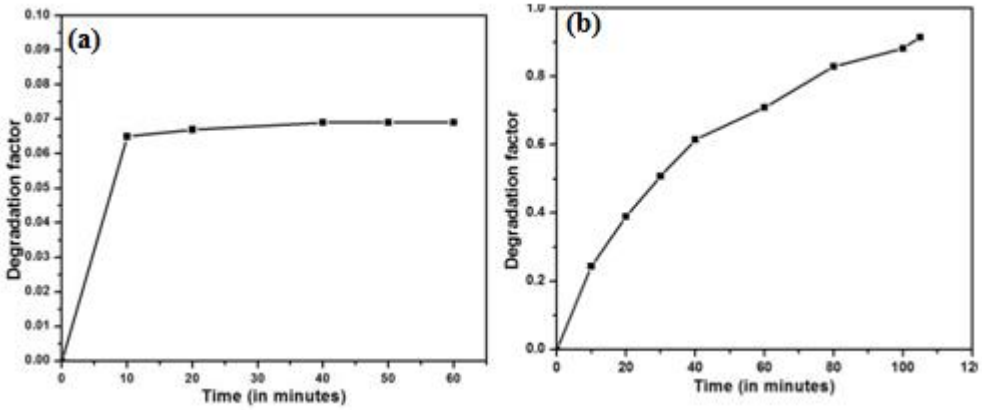

Fig. 4.7 Degradation factor vs time plots of (a) (a) in absence of catalyst, (b) in presence of SG

The degradation of MV with *m*-ZrO_2/$rGO_{600^\circ C}$, *m*-ZrO_2/$rGO_{1000^\circ C}$, *m*-ZrO_2/$rGO_{1200^\circ C}$ and *m*-ZrO_2/$SG_{1200^\circ C}$ catalyst in presence of visible light was carried out. Their UV spectrum and corresponding degradation factor versus time plots are shown in Fig.4.8 and Fig.4.9 respectively. With increasing annealing temperature degradation time decreases. The degradation time for *m*-ZrO_2/$rGO_{600^\circ C}$, *m*-ZrO_2/$rGO_{1000^\circ C}$, *m*-ZrO_2/$rGO_{1200^\circ C}$ and *m*-ZrO_2/$SG_{1200^\circ C}$ are 50 min, 45 min, 25 min and 8 min, respectively. The degradation and % degradation values for the various photo-catalysts are shown in table 4.2.

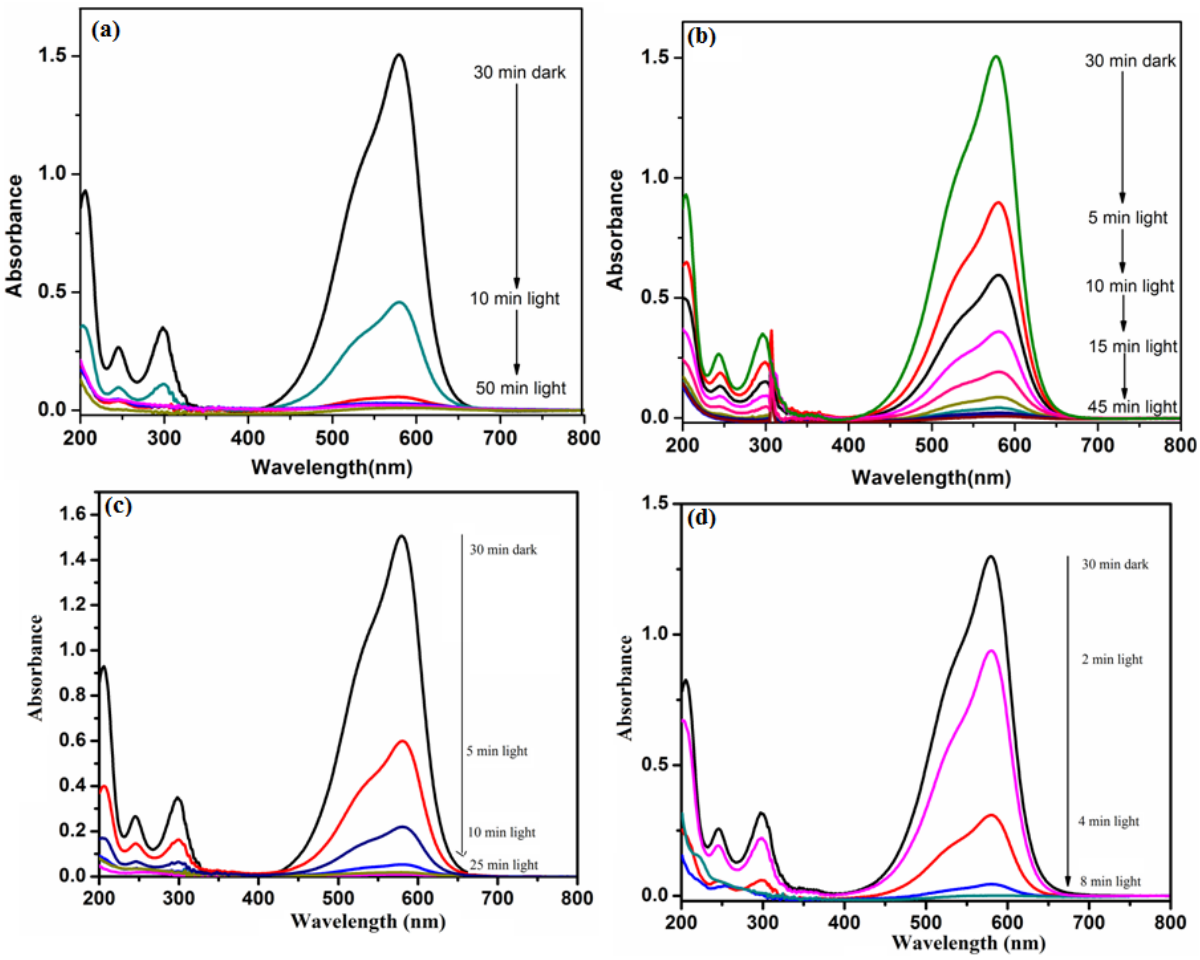

Fig. 4.8 UV spectrum of photocatalytic degradation of MV by (a) *m*-ZrO_2/$rGO_{600^\circ C}$, (b) *m*-ZrO_2/$rGO_{1000^\circ C}$, (c) *m*-ZrO_2/$rGO_{1200^\circ C}$ and (d) *m*-ZrO_2/$SG_{1200^\circ C}$

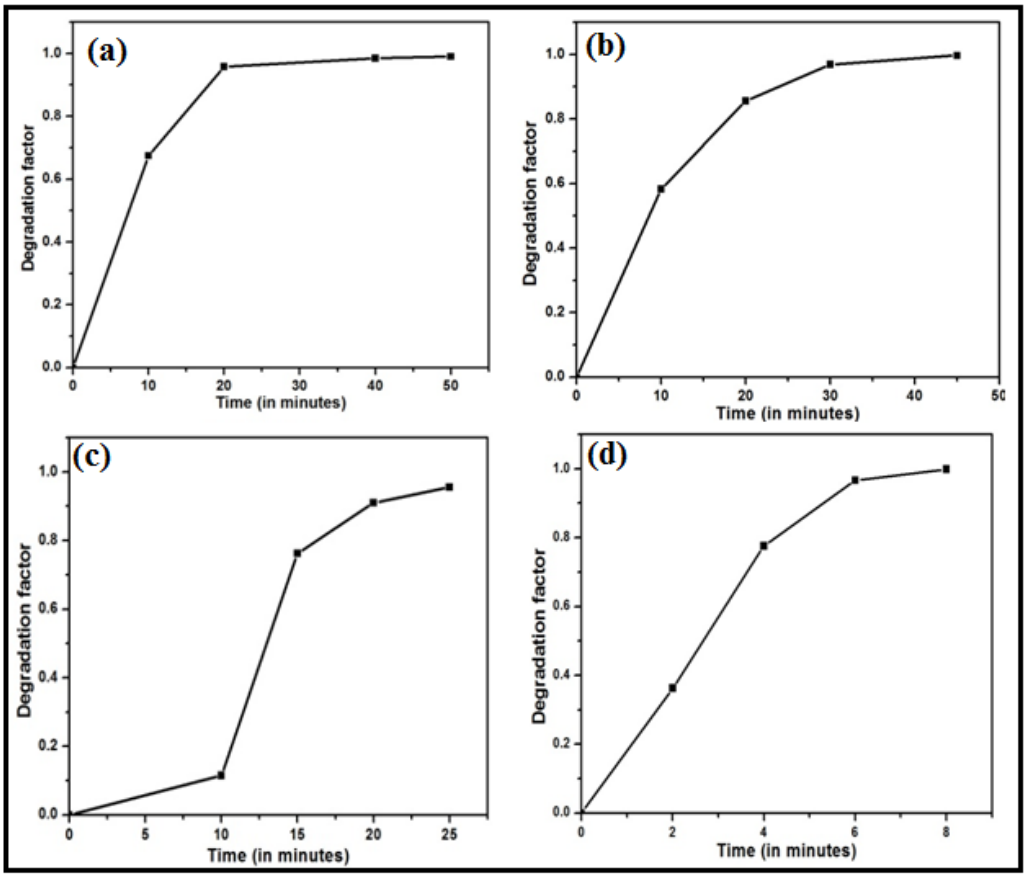

Fig. 4.9 Degradation factor vs time (minutes) plots for (a) *m*-ZrO_2/$rGO_{600^\circ C}$, (b) *m*-ZrO_2/$rGO_{1000^\circ C}$, (c) *m*-ZrO_2/$rGO_{1200^\circ C}$ and (d) *m*-ZrO_2/$SG_{1200^\circ C}$

Table 4.2 Degradation of MV in presence of catalyst

Photocatalyst	Degradation time (in minutes)	Degradation factor (%)
SG	100	91.5
***m*-ZrO_2/$rGO_{600^\circ C}$**	50	99.1
***m*-ZrO_2/$rGO_{1000^\circ C}$**	45	99.7
***m*-ZrO_2/$rGO_{1200^\circ C}$**	25	99.8
***m*-ZrO_2/$SG_{1200^\circ C}$**	8	99.9

It was clearly observed that the incorporation of ZrO_2 onto the surface of rGO and SG has increased its photo catalytic activities. It was also observed that the photo catalytic activity shows strong dependence on the irradiation time and degradation increases with increase in irradiation time. ZrO_2 surface gain more energy from light at higher exposure time, and due to this reason the degradation of MV was increased with

time. The photo degradation of MV was increased with increasing annealing temperatures. This effect may be observed due to decrease in band gap of ZrO_2 with increase in annealing temperature, reduction in recombination centers and improved crystallinity at higher temperatures. This decrease in band gap was correlated with grains size increases with temperature, when the latter increases the defects and impurities tend to disappear causing a reorganization of the structure. The presence of single monoclinic phase also enhanced the photo catalytic activity which acts as active sites for photo degradation. *m*-ZrO_2/ $SG_{1200^\circ C}$ shows lowest degradation time as well as highest degradation factor which may be due to the enhanced adsorptivity of SG. SG can bind dye molecules through π-π conjugated stacking and hence increase the adsorptivity.

4.3.6 Recyclization and reuse of m-ZrO_2*/*$SG_{1200^\circ C}$

In order to investigate the stability of the photocatalyst after one use, recyclization of *m*-ZrO_2/$SG_{1200^\circ C}$ catalyst was performed. The photocatalytic degradation reaction was carried out in visible light for 8 minutes. After each cycle the catalyst was washed with absolute alcohol and distilled water. A significant degradation occurred for the first three cycles. After the third cycle, the degradation seemed to decrease i.e. the concentration of the MV solution did not decrease significantly. This may be due to the loss of the catalyst while washing with alcohol and distilled water for several times. The change in concentration of dye with no. of cycles is shown in Fig.4.9.

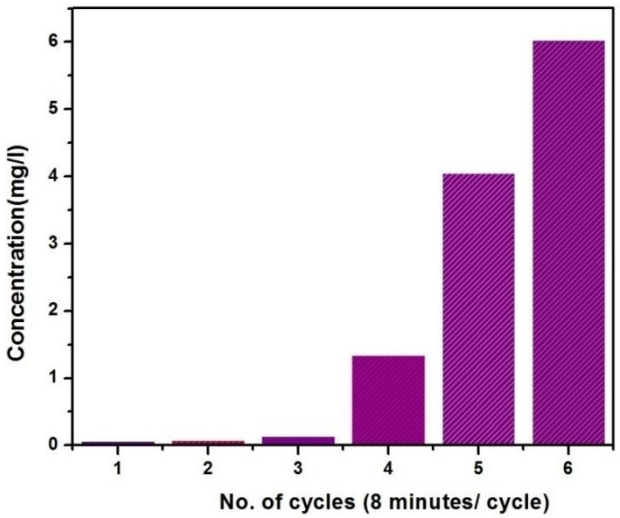

Fig. 4.10 Column graph showing change in concentration of undegraded MV solution versus number cycles.

4.4 Conclusion

In this study, it was seen that the incorporation of ZrO_2 into graphene and sulfonated graphene has increased its photo-catalytic activity. The photo-catalytic activity of ZrO_2 also increases with the increase in annealing temperatures. Thus, the *m*-ZrO_2/SG $_{1200^{\circ}C}$ catalyst was observed to possess the highest catalytic efficiency amongst the other synthesized materials. This effect may be observed due to decrease in band gap of ZrO_2 with increase in annealing temperature, reduction in recombination centers and improved crystallinity at higher temperatures. This photocatalyst can be used for successful dye degradation or removal of dyes from waste water. The photocatalyst can also be regenerated and reused after washing it.

4.5 References

[1] Sarkar, C., Bora, C., and Dolui, S. K. Selective dye adsorption by pH modulation on amine-functionalized reduced graphene oxide-carbon nanotube hybrid. *Industrial & Engineering Chemistry Research*, 53(42):16148-16155, 2014.

[2] Ramesha, G. K., Kumara, A. V., Muralidhara, H. B., and Sampath, S. Graphene and graphene oxide as effective adsorbents toward anionic and cationic dyes. *Journal of colloid and interface scienc*e, 361(1):270-277, 2011.

[3] Shi, B., Li, G., Wang, D., Feng, C., and Tang, H. Removal of direct dyes by coagulation: The performance of preformed polymeric aluminum species. *Journal of hazardous materials*, 143(1-2):567-574, 2007.

[4] Khan, R., Bhawana, P., and Fulekar, M. H. Microbial decolorization and degradation of synthetic dyes: a review. *Reviews in Environmental Science and Bio/Technology*, 12(1):75-97, 2013.

[5] Lachheb, H., Puzenat, E., Houas, A., Ksibi, M., Elaloui, E., Guillard, C., and Herrmann, J.M. Photocatalytic degradation of various types of dyes (Alizarin S, Crocein Orange G, Methyl Red, Congo Red, Methylene Blue) in water by UV-irradiated titania. *Applied Catalysis B: Environmental*, 39(1):75-90, 2002.

[6] Lachheb, H., Puzenat, E., Houas, A., Ksibi, M., Elaloui, E., Guillard, C., and Herrmann, J.M. Photocatalytic degradation of various types of dyes (Alizarin S, Crocein Orange G, Methyl Red, Congo Red, Methylene Blue) in water by UV-irradiated titania. *Applied Catalysis B: Environmental*, 39(1):75-90, 2002.

[7] Xu, F., Shen, Y., Sun, L., Zeng, H., and Lu, Y. Enhanced photocatalytic activity of hierarchical ZnO nanoplate-nanowire architecture as environmentally safe and facilely recyclable photocatalyst. *Nanoscale*, 3(12):5020-5025, 2011.

[8] Chong, M. N., Jin, B., Chow, C. W., and Saint, C. Recent developments in photocatalytic water treatment technology: a review. *Water research*, 44(10):2997-3027, 2010.

[9] Dapeng, L.I. and Jiuhui, Q.U. The progress of catalytic technologies in water purification: A review. *Journal of Environmental Sciences*, 21(6):713-719, 2009.

[10] Xiang, Q., Yu, J., and Jaroniec, M. Graphene-based semiconductor photocatalysts. *Chemical Society Reviews*, 41(2):782-796, 2012.

[11] Xiang, Q., Yu, J., and Wong, P. K. Quantitative characterization of hydroxyl radicals produced by various photocatalysts. *Journal of Colloid and Interface Science*, 357(1):163-167, 2011.

[12] Liu, B., Hu, J., and Foord, J. S. Electrochemical deposition of zirconia films on diamond electrodes. *Electrochemical and Solid-State Letters*, 14(2):D20-D22, 2011.

[13] Vilian, A. E., Chen, S. M., Ali, M. A., and Al-Hemaid, F. M. Direct electrochemistry of glucose oxidase immobilized on ZrO_2 nanoparticles-decorated reduced graphene oxide sheets for a glucose biosensor. *RSC Advances*, 4(57):30358-30367, 2014.

[14] Kauppi, E. I., Rönkkönen, E. H., Airaksinen, S. M., Rasmussen, S. B., Bañares, M. A., and Krause, A. O. I. Influence of H_2S on ZrO_2-based gasification gas clean-up catalysts: MeOH temperature-programmed reaction study. *Applied Catalysis B: Environmental*, 111:605-613, 2012.

[15] Signoretto, M., Menegazzo, F., Contessotto, L., Pinna, F., Manzoli, M., and Boccuzzi, F Au/ZrO_2: an efficient and reusable catalyst for the oxidative esterification of renewable furfural. *Applied Catalysis B: Environmental*, 129:287-293, 2013.

[16] Zhang, W., Cui, Y., Hu, Z. G., Yu, W. L., Sun, J., Xu, N., Ying, Z. F., and Wu, J.D. Structural, optical and electrical properties of high-k ZrO_2 dielectrics on Si prepared by plasma assisted pulsed laser deposition. *Thin Solid Films*, 520(20):6361-6367, 2012.

[17] Wang, Y., Liu, J., and Guo, A. Moderate temperature compression incorporating plastic deformation and rearrangement in Al_2O_3–ZrO_2 ceramics. *Ceramics International*, 39(1):883-886, 2013.

[18] Zhang, R., Zhang, X., and Hu, S. High temperature and pressure chemical sensors based on Zr/ZrO_2 electrode prepared by nanostructured ZrO_2 film at Zr wire. *Sensors and Actuators B: Chemical*, 149(1):143-154, 2010.

[19] Sun, W., Zhang, N., Mao, Y., and Sun, K. Preparation of dual-pore anode supported Sc_2O_3-stabilized-ZrO_2 electrolyte planar solid oxide fuel cell by phase-inversion and dip-coating. *Journal of Power Sources*, 218:352-356, 2012.

[20] Ashkarran, A. A., Afshar, S. A. A., and Aghigh, S. M. Photocatalytic activity of ZrO_2 nanoparticles prepared by electrical arc discharge method in water. *Polyhedron*, 29(4):1370-1374, 2010.

[21] Navio, J. A., Hidalgo, M. C., Colon, G., Botta, S. G., and Litter, M. I. Preparation and physicochemical properties of ZrO_2 and Fe/ZrO_2 prepared by a sol− gel technique. *Langmuir*, 17(1):202-210, 2001.

[22] Botta, S. G., Navío, J. A., Hidalgo, M. C., Restrepo, G. M., and Litter, M. I. Photocatalytic properties of ZrO_2 and Fe/ZrO_2 semiconductors prepared by a sol–gel technique. *Journal of Photochemistry and Photobiology A: Chemistry*, 129(1-2):89-99, 1999.

[23] Sayama, K. and Arakawa, H. Photocatalytic decomposition of water and photocatalytic reduction of carbon dioxide over zirconia catalyst. *The Journal of Physical Chemistry*, 97(3):531-533, 1993.

[24] Basahel, S. N., Ali, T. T., Mokhtar, M., and Narasimharao, K. Influence of crystal structure of nanosized ZrO_2 on photocatalytic degradation of methyl orange. *Nanoscale research letters*, 10(1):73, 2015.

[25] Yu, Y., Zhang, P., Kuang, Y., Ding, Y., Yao, J., Xu, J., and Cao, Y. Adjustment and Control of Energy Levels for TiO_2–N/ZrO_2–x N x with Enhanced Visible Light Photocatalytic Activity. *The Journal of Physical Chemistry C*, 118(36):20982-20988, 2014.

[26] Xiang, Q., Yu, J., and Jaroniec, M. Graphene-based semiconductor photocatalysts. *Chemical Society Reviews*, 41(2):782-796, 2012.

[27] Zhu, M., Chen, P., and Liu, M. Ag/AgBr/graphene oxide nanocomposite synthesized via oil/water and water/oil microemulsions: a comparison of sunlight energized plasmonic photocatalytic activity. *Langmuir*, 28(7):3385-3390, 2012.

[28] Shah, M. S. A. S., Zhang, K., Park, A. R., Kim, K. S., Park, N. G., Park, J. H., and Yoo, P. J. Single-step solvothermal synthesis of mesoporous Ag-TiO_2-reduced graphene oxide ternary composites with enhanced photocatalytic activity. *Nanoscale*, 5(11):5093-5101, 2013.

[29] Nipane, S. V., Korake, P. V., and Gokavi, G. S. Graphene-zinc oxide nanorod nanocomposite as photocatalyst for enhanced degradation of dyes under UV light irradiation. *Ceramics International*, 41(3):4549-4557, 2015.

[30] Zhang, Y., Tang, Z. R., Fu, X., and Xu, Y. J. TiO_2-graphene nanocomposites for gas-phase photocatalytic degradation of volatile aromatic pollutant: is TiO_2-graphene truly different from other TiO_2-carbon composite materials?. *ACS nano*, 4(12):7303-7314, 2010.

[31] Du, D., Liu, J., Zhang, X., Cui, X., and Lin, Y One-step electrochemical deposition of a graphene-ZrO_2 nanocomposite: preparation, characterization and application for detection of organophosphorus agents. *Journal of Materials Chemistry*, 21(22):8032-8037, 2011.

[32] Zhao, G., Jiang, L., He, Y., Li, J., Dong, H., Wang, X., and Hu, W. Sulfonated graphene for persistent aromatic pollutant management. *Advanced materials*, 23(34):3959-3963, 2011.

[33] Coşkun, E., Zaragoza-Contreras, E. A., and Salavagione, H. J. Synthesis of sulfonated graphene/polyaniline composites with improved electroactivity. *Carbon*, 50(6):2235-2243, 2012.

[34] Wang, L., Wang, D., Zhang, S., and Tian, H. Synthesis and characterization of sulfonated graphene as a highly active solid acid catalyst for the ester-exchange reaction. *Catalysis Science & Technology*, 3(5):1194-1197, 2013.

[35] Ji, J., Zhang, G., Chen, H., Wang, S., Zhang, G., Zhang, F., and Fan, X. Sulfonated graphene as water-tolerant solid acid catalyst. *Chemical Science*, 2(3):484-487, 2011.

[36] Lee, J. S., You, K. H. and Park, C. B. Highly photoactive, low bandgap TiO_2 nanoparticles wrapped by graphene. *Advanced Materials*, 24(8):1084-1088, 2012.

[37] Rani, S., Kumar, M., Sharma, S., Kumar, D., and Tyagi, S. Effect of graphene in enhancing the photo catalytic activity of zirconium oxide. *Catalysis letters*, 144(2):301-307, 2014.

[38] Gurushantha, K., Anantharaju, K. S., Renuka, L., Sharma, S. C., Nagaswarupa, H. P., Prashantha, S. C., Vidya, Y. S., and Nagabhushana, H. New green synthesized reduced graphene oxide-ZrO_2 composite as high performance photocatalyst under sunlight. *RSC Advances*, 7(21):12690-12703, 2017.

[39] William, S., Hummers, J. R., and Offeman, R. E. Preparation of graphitic oxide. *Journal of the American Chemical Society*, 80(6):1339-1339, 1958.

[40] Si, Y. and Samulski, E. T. Synthesis of water soluble graphene. *Nano letters*, 8(6):1679-1682, 2008.